Chapter 33

NONLINEAR METHODS AND CHAOS

Our mind would lose itself in the complexity of the world if that complexity were not harmonious; like the short-sighted, it would only see the details, and would be obliged to forget each of these details before examining the next, because it would be incapable of taking in the whole. The only facts worthy of our attention are those which introduce order into this complexity and so make it accessible to us. HENRI POINCARÉ

The origin of nonlinear dynamics goes back to the work of the renowned French mathematician Henri Poincaré on celestial mechanics at the turn of the twentieth century. Classical mechanics is, in general, nonlinear in its dependence on the coordinates of the particles and the velocities; one example being vibrations with a nonlinear restoring force. The Navier-Stokes equations are nonlinear, which makes hydrodynamics difficult to handle. For almost four centuries however, following the lead of Galileo, Newton, and others, physicists have focused on predictable, effectively linear responses of classical systems, which usually have linear and nonlinear properties.

Poincaré was the first to understand the possibility of completely irregular, or "chaotic," behavior of solutions of nonlinear differential equations that are characterized by an extreme sensitivity to initial conditions: Given slightly different initial conditions, from errors in measurements for example, solutions can grow exponentially apart with time, so the system soon becomes effectively unpredictable, or "chaotic." This property of chaos, often called the "butterfly" effect, will be discussed in subsequent sections of this chapter, with its first illustration in Section 33.1. Since the rediscovery of this effect by Lorenz in meteorology in the early 1960s, the field of nonlinear dynamics has grown tremendously. Thus, nonlinear dynamics and chaos theory now have entered the mainstream of physics.

Numerous examples of nonlinear systems have been found to display irregular behavior. Surprisingly, order, in the sense of quantitative similarities as universal properties, or other regularities may arise spontaneously in chaos; a first example is Feigenbaum's universal number δ, which appears in Section 33.1. Dynamical chaos is not a rare phenomenon but is ubiquitous in nature. It includes irregular shapes of clouds, coast lines, and other landscapes, which are examples of fractals, to be discussed in Section 33.3, and turbulent flow of fluids, water dripping from a faucet,

and of course, the weather. The damped, driven pendulum is among the simplest systems displaying chaotic motion.

It has been shown that necessary conditions for chaotic motion in dynamical systems described by **first-order** differential equations are

- at least three dynamical variables, and
- one or more nonlinear terms coupling two or several of them.

A central theme in chaos is the evolution of **complex** forms from the repetition of **simple** but **nonlinear** operations; this is being recognized as a **fundamental organizing principle of nature**. While nonlinear differential equations are a natural place in physics for chaos to occur, the mathematically simpler iteration of nonlinear functions provides a quicker entry to chaos theory, which we will pursue first in Section 33.1. In this context, chaos already arises in certain nonlinear functions of a **single** variable.

33.1 THE LOGISTIC MAP

The nonlinear one-dimensional iteration, or difference equation,

$$x_{n+1} = \mu x_n(1 - x_n) \,, \qquad 1 < \mu < 4, \tag{33.1}$$

is called the **logistic map**. In fact, the term **map** is used to identify discrete iterative systems that may be more general than the present example. Equation (33.1) permits the generation of a set of values x_i from a starting, or initial value x_0, and is is patterned after the nonlinear differential equation $dx/dt = \mu x(1 - x)$, used by P. F. Verhulst in 1845 to model the development of a breeding population whose generations do not overlap. The density of the population at time n is x_n. The linear term simulates the birth rate and the nonlinear term the death rate of the species in a constant environment controlled by the parameter μ.

The quadratic function $f_\mu(x) = \mu x(1 - x)$ is chosen because it has one maximum in the interval $[0, 1]$ and is zero at the endpoints, $f_\mu(0) = 0 = f_\mu(1)$. In addition, $f_\mu(x)$ is symmetric about $x = 1/2$, where it has the maximum value

$$f_\mu(1/2) = \frac{\mu}{4} \,. \tag{33.2}$$

By imposing the requirement $\mu < 4$, we assure that the iterative process of Eq. (33.1) with $0 < x_0 < 1$ will produce x_i that also remain within that range. The requirement $\mu > 1$ is imposed so that the sequences generated by Eq. (33.1) will not always tend to zero and therefore be "uninteresting".

Our main concern will be the behavior that our difference equation exhibits in the limit of large numbers of iterations, and in particular the way in which the values chosen for the parameter μ and the "input" x_0 effect the outcome. We will find that

- Varying the single parameter μ controls a rich and complex behavior, including one-dimensional chaos. More parameters or additional variables are hardly necessary at this point to provide a meaningful illustration. In a rather qualitative sense the simple **logistic map** of Eq. (33.1) is representative of many dynamical systems in biology, chemistry, and physics.

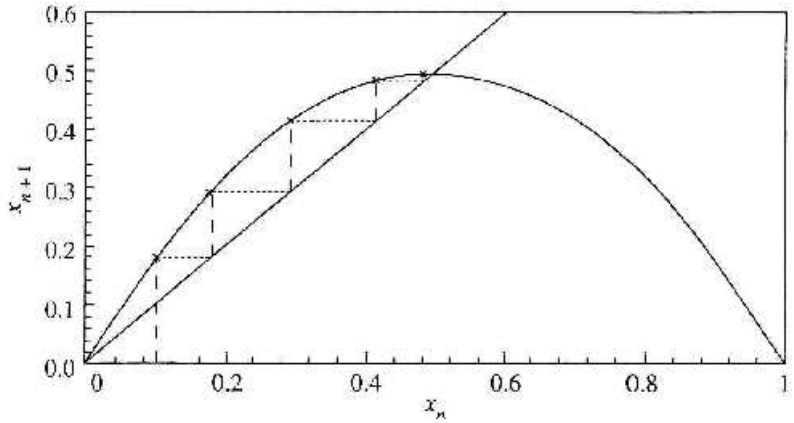

Figure 33.1: Cycle $(x_0, x_1, \ldots)$ for the logistic map for $\mu = 2$, starting value $x_0 = 0.1$ and attractor $x^* = 1/2$.

Figure 33.1 shows a plot of $f_\mu(x) = \mu x(1-x)$ for $\mu = 2$ along with the diagonal and a series of points $(x_0, x_1, \ldots)$ that result from repeated application of Eq. (33.1), starting from the chosen value $x_0 = 0.1$. This series of x_i is called a **cycle**; that name implies periodic repetition though in the present case what we actually have here is a sequence that converges unidirectionally to the limit $x^* = 1/2$. The cycle can be constructed graphically. By drawing a vertical line at $x = x_0$, its intersection with the curve for f_μ identifies $f_\mu(x_0)$; a horizontal line through the intersection intersects the diagonal at the x value $x_1 = f_\mu(x_0)$. Then we draw a vertical line at $x = x_1$ to find $f_\mu(x_1)$ and a horizontal line from $f_\mu(x_1)$ to locate x_2. Continuing this process through additional iterations, Fig. 33.1 shows how it converges to a limit point which we designate x^*. From the graph it appears that $x^* = 0.5$.

If we start from any other initial value x_0 in the range $0 < x_0 < 1$ we obtain the same limiting result, namely that the x_i converge toward the same point $x^* = 0.5$. We can compute this value of x^* because it must satisfy

$$f_\mu(x^*) = \mu x^*(1-x^*) = x^* \ , \quad \text{with solution} \quad x^* = 1 - \frac{1}{\mu} \ , \tag{33.3}$$

for $\mu = 2$ confirming our result $x^* = 0.5$. Equation (33.3) has another solution, $x^* = 0$, but that solution is only reached in the uninteresting case $x_0 = 0$. The two solutions of Eq. (33.3) are called **fixed points** of the map.

If now we consider applying Eq. (33.1) for x_0 values outside the range $0 < x_0 < 1$, the behavior is quite different. For both $x_0 < 0$ and $x_0 > 1$, x_1 and all x_i with $i > 1$ are negative, and our cycle diverges with $x_i \to -\infty$. We describe the behavior of our iterative system by identifying the point $x^* = 0.5$ as an **attractor**, namely a fixed point with a **basin of attraction** which is the interval $0 < x < 1$; we identify the fixed point $x = 0$ as a **repellor**. Thus, a cycle starting from x_0 will move away from $x = 0$, and (if x_0 is in the basin of attraction) toward $x = 0.5$.

Whether a fixed point is an attractor or a repellor is determined by the slope of f_μ at the fixed point. To see this, we expand $f_\mu(x_n)$ about the fixed point x^*, obtaining

$$x_{n+1} = f_\mu(x_n) = f_\mu(x^*) + f'_\mu(x^*)(x_n - x^*) + \cdots \ .$$

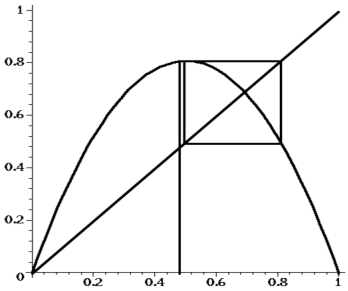

Figure 33.2: Cycle $(0.495, 0.812)$ for the logistic map for $\mu = 3.25$, starting from $x_0 = 0.48$.

Remembering that $f_\mu(x^*) = x^*$, this equation yields, to first order,

$$\frac{x_{n+1} - x^*}{x_n - x^*} = f'_\mu(x^*) = \mu(1 - 2x^*) \; .$$

If x_n is sufficiently close to x^* that a first-order estimate is valid, we see that if $|f'_\mu(x^*)| < 1$, then the next iterate, x_{n+1} will lie closer to x^* than does x_n, implying that the iterative process will approach x^*, which must then be an **attractor**. On the other hand, if $|f'_\mu(x^*)| > 1$, then x_{n+1} will lie further from x^* than did x_n, and the fixed point will then be a **repellor**. At the fixed point $x^* = 0$, we have $f'_\mu(0) = \mu$, which exceeds unity for the entire range $1 < \mu < 4$, so (as expected) $x^* = 0$ is for all μ a repellor. For the "interesting" fixed point $x^* = 1 - \mu^{-1}$, we have

$$f'(x^*) = \mu[1 - 2(1 - \mu^{-1})] = 2 - \mu \; .$$

We thus see that this fixed point will be an attractor for $\mu < 3$, and a repellor for $\mu > 3$.

BIFURCATIONS AND CHAOS

For $\mu > 3$ the situation is actually more complicated than may be apparent from the foregoing discussion; the limiting behavior of the iterative process (for large n) is that the values of the x_n alternate between two points which we call **fixed points of period 2**. This strange behavior is illustrated by the following sequence of x_i for $\mu = 3.25$, starting from $x_0 = 0.80$:

$x_1 = 0.52000$	$x_5 = 0.49515$	$x_9 = 0.49526$	$x_{13} = 0.49527$
$x_2 = 0.81120$	$x_6 = 0.81242$	$x_{10} = 0.81243$	$x_{14} = 0.81243$
$x_3 = 0.49775$	$x_7 = 0.49527$	$x_{11} = 0.49527$	$x_{15} = 0.49527$
$x_4 = 0.81248$	$x_8 = 0.81243$	$x_{12} = 0.81243$	$x_{16} = 0.81243$

It is clear that we return to each of the fixed points (0.81243 and 0.49527) at intervals of **two iterations**. To picture this limiting behavior graphically, we may draw a diagram using the construction that led to Fig. 33.1; the result (obtained when x_0 is chosen as the fixed point 0.49527) is the periodic pattern shown in Fig. 33.2.

Figure 33.3 shows a graph plotting these (and other fixed points of the logistic map) as a function of μ. The graph shows that there is a single fixed point up

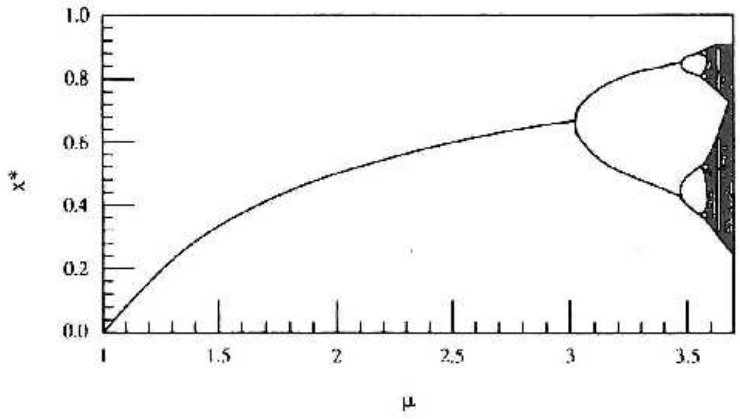

Figure 33.3: Bifurcation plot for the logistic map: Fixed points x^* versus μ.

to $\mu = 3$, where it **bifurcates**, or splits, into the curves describing the two points between which the iterations alternate (in the limit of large n). This splitting is called a **pitchfork** bifurcation because of its characteristic (rounded-Y) shape. Notice that our simple, but nonlinear difference equation is capable of generating a sudden change in the evolution of the system as μ is changed continuously.

We can locate these fixed points of period 2 (designated x_2^*) by solving

$$x_2^* = f_\mu(f_\mu(x_2^*)) = \mu^2 x_2^*(1-x_2^*)\Big[1-\mu x_2^*(1-x_2^*)\Big] \tag{33.4}$$

for x_2^*. After dividing Eq. (33.4) through by x_2^*, we have left a cubic equation. However, we know one of its three roots, namely the quantity we labelled x^* (which is for $\mu > 3$ a repellor and will therefore not be a limit point of the iteration in x_n). Using this information, we may bring Eq. (33.4) to the factored form

$$0 = (x_2^* - 1 + \mu^{-1})\left[\mu + 1 - \mu(\mu+1)x_2^* + \mu^2 (x_2^*)^2\right] \ . \tag{33.5}$$

The part of Eq. (33.5) that is in square brackets has the two roots

$$x_2^* = \frac{1}{2\mu}\left(\mu + 1 \pm \sqrt{(\mu+1)(\mu+3)}\right) \ , \tag{33.6}$$

which are the two branches in Fig. 33.3 that start at $\mu = 3$, $x^* = 2/3$. These points will be attractors (of period 2) in the range of μ where $f_\mu(f_\mu(x))$ has at $x = x_2^*$ a first derivative of magnitude less than unity. It can be shown that this derivative, which is unity at $\mu = 3$, decreases with increasing μ. However, when μ reaches $1 + \sqrt{6} \approx 3.44949$, the derivative of $f_\mu(f_\mu(x))$ will (for both branches of x_2^*) reach the value -1, and both branches will themselves bifurcate, leading for μ greater than approximately 3.44949 to a set of four limiting values for x_n which will (at large n) be reached in succession with iteration in n. This **period doubling** occurs at $x_2^* = 0.43996$ and $x_2^* = 0.849938$. This behavior is illustrated by the following data

for $\mu = 3.53$, starting from $x_0 = 0.517$:

$x_1 = 0.88148$	$x_5 = 0.88147$	$x_9 = 0.88148$	$x_{13} = 0.88147$
$x_2 = 0.36879$	$x_6 = 0.36883$	$x_{10} = 0.36880$	$x_{14} = 0.36882$
$x_3 = 0.82173$	$x_7 = 0.82176$	$x_{11} = 0.82174$	$x_{15} = 0.82175$
$x_4 = 0.51711$	$x_8 = 0.51704$	$x_{12} = 0.51709$	$x_{16} = 0.51705$

As μ is further increased, additional period doublings occur, and it becomes impossible to obtain analytic solutions. However, iterations are easily done numerically on a programmable pocket calculator or a personal computer, whose rapid improvements (computer-driven graphics, in particular) and wide distribution in the 1970s has accelerated the development of chaos theory. The sequence of bifurcations continues with ever longer periods until we reach $\mu_\infty = 3.5699456\cdots$, where an infinite number of bifurcations occurs. Near bifurcation points, fluctuations and rounding errors in initial conditions play an increasing role because the system has to choose between two possible branches and becomes much more sensitive to small perturbations. The bands of fixed points x^* begin forming a continuum (shown dark in Fig. 33.3); this is where chaos starts. Within the chaotic region, the x_n never repeat.

This increasing period doubling that is the route to chaos for the logistic map can be characterized by the ratios of their spacings in μ. Letting μ_i denote the μ values where bifurcations occur, so that $\mu_1 = 3$, $\mu_2 = 3.45\cdots$, etc., it has been shown that these ratios approach the limit

$$\lim_{n\to\infty} \frac{\mu_n - \mu_{n-1}}{\mu_{n+1} - \mu_n} = \delta = 4.66920161\cdots . \tag{33.7}$$

The first three bifurcations in Fig. 33.3 yield a fairly crude approximation to the limit:

$$\frac{\mu_2 - \mu_1}{\mu_3 - \mu_2} = \frac{3.45 - 3.00}{3.54 - 3.45} = 5.0 .$$

It has also been shown that this limit, known as the **Feigenbaum number** of the mapping defined by $f_\mu(x)$, is a constant whose value depends only on the behavior of $f_\mu(x)$ in the neighborhood of its maximum. If near x_m, $f(x) \approx f(x_m) - |x - x_m|^{1+\varepsilon}$ for some ε between 0 and 1, the Feigenbaum number has a value that depends only upon ε: for quadratic maps ($\varepsilon = 1$), δ has the value given in Eq. (33.7); for linear maps ($\varepsilon = 0$), $\delta = 2$.[1]

The Feigenbaum number is an example of order in chaos. Experience shows that its validity is even wider than illustrated here, including two-dimensional (dissipative) systems and twice continuously differentiable functions with subharmonic bifurcations.[2]

Finally, we note that the behavior of the logistic map is even more complicated than has been revealed by the above discussion. At several points within the chaotic region that begins at μ_∞, the system temporarily becomes periodic again; the largest of these regions begins with a cycle of period 3 at $\mu \approx 3.8282$.

[1] For other maps and a discussion of the fascinating history how chaos became again a hot research topic, see D. Holton and R. M. May in *The Nature of Chaos* (T. Mullin, ed.), Oxford, UK: Clarendon Press (1993), Section 5, p. 95; and Gleick's *Chaos* in Additional Readings.

[2] More details and computer codes for the logistic map are given by G. L. Baker and J. P. Gollub (see Additional Readings).

LYAPUNOV EXPONENTS

Earlier in this section we described how, as we approach the period-doubling accumulation parameter value $\mu_\infty = 3.5699\cdots$ from below, the period $n+1$ of cycles (x_0, x_1, …, x_n) with $x_{n+1} = x_0$ gets longer. Letting $f^{(n)}$ stand for the n-fold iteration of f_μ, i.e. $f^{(2)}(x) = f_\mu(f_\mu(x))$ etc, it is also easy to check that the distances d_n between the n-th iterates of sequences that started separated by only a small difference $\varepsilon > 0$ in x_0,

$$d_n = |f^{(n)}(x_0 + \varepsilon) - f^{(n)}(x_0)| \,, \tag{33.8}$$

grow rapidly. Remember that $f^{(n)}$ stands for an n-fold iteration and not for an n-th derivative. From experience with chaotic behavior we find that this distance increases exponentially as $n \to \infty$; that is, $d_n/\varepsilon = e^{\lambda n}$, or

$$\lambda = \lim_{n\to\infty} \frac{1}{n} \ln\left(\frac{|f^{(n)}(x_0 + \varepsilon) - f^{(n)}(x_0)|}{\varepsilon}\right). \tag{33.9}$$

We call λ the **Lyapunov exponent** for the cycle. For $\varepsilon \to 0$ we may rewrite Eq. (33.9) in terms of derivatives as

$$\lambda = \lim_{n\to\infty} \frac{1}{n} \ln\left|\frac{df^{(n)}(x_0)}{dx}\right| = \lim_{n\to\infty} \frac{1}{n} \sum_{i=0}^{n} \ln|f'(x_i)| \,. \tag{33.10}$$

To obtain the result in Eq. (33.10) we used the chain rule of differentiation for $df^{(n)}(x)/dx$, so

$$\frac{df^{(2)}(x_0)}{dx} = \left.\frac{df_\mu}{dx}\right|_{x=f_\mu(x_0)} \left.\frac{df_\mu}{dx}\right|_{x=x_0} = f'_\mu(x_1) f'_\mu(x_0) \,, \tag{33.11}$$

and the extension to $df^{(n)}/dx$ is obvious. Our Lyapunov exponent has been calculated at the point x_0, and Eq. (33.10) is exact for one-dimensional maps.

As a measure of the sensitivity of the system to changes in initial conditions, one point is not enough to determine λ in higher-dimensional dynamical systems in general. In such cases, we repeat the procedure for several points on the trajectory and average over them. This way, we obtain the **average Lyapunov exponent** for the sample. This average value is often called and taken as the Lyapunov exponent.

The Lyapunov exponent λ is a quantitative measure of chaos: A one-dimensional iterated function similar to the logistic map has **chaotic** cycles (x_0, x_1, …) **if the average Lyapunov exponent is positive** for that value of μ. Any such initial point x_0 is then called a **strange** or **chaotic attractor** (the shaded region in Fig. 33.3). For cycles of finite period, λ is negative. This is the case for $\mu < \mu_\infty$, and even in the periodic windows at larger μ (such as that near $\mu = 3.8282$). At bifurcation points, $\lambda = 0$. For $\mu > \mu_\infty$ the Lyapunov exponent is positive, except in the periodic windows, where $\lambda < 0$, and λ grows with μ. In other words, the system becomes more chaotic as the control parameter μ increases.

In the chaos region of the logistic map there is a scaling law for the average Lyapunov exponent (we do not derive it),

$$\lambda(\mu) = \lambda_0(\mu - \mu_\infty)^{\ln 2/\ln\delta}, \tag{33.12}$$

where $\ln 2/\ln\delta \sim 0.445$, δ is the universal Feigenbaum number of Eq. (33.7), and λ_0 is a constant. This relation, Eq. (33.12), is reminiscent of the formulas that describe

physical observables at a (second-order) phase transition. The exponent in Eq. (33.12) is a universal number; the Lyapunov exponent plays the role of an **order parameter**, while $\mu - \mu_\infty$ is the analog of $T - T_c$, where T_c is the **critical** temperature at which the phase transition occurs.

Exercises

33.1.1. Show that $x^* = 1$ is a nontrivial fixed point of the map $x_{n+1} = x_n \exp[r(1-x_n)]$ with a slope $1 - r$, so that the equilibrium is stable if $0 < r < 2$.

33.1.2. Draw a bifurcation diagram for the exponential map of Exercise 33.1.1 for $r > 1.9$.

33.1.3. Determine fixed points of the cubic map $x_{n+1} = ax_n^3 + (1-a)x_n$ for $0 < a < 4$ and $0 < x_n < 1$.

33.1.4. Write the time-delayed logistic map $x_{n+1} = \mu x_n(1-x_{n-1})$ as a two-dimensional map: $x_{n+1} = \mu x_n(1-y_n)$, $y_{n+1} = x_n$, and determine some of its fixed points.

33.1.5. Show that the second bifurcation for the logistic map that leads to cycles of period 4 is located at $\mu = 1 + \sqrt{6}$.

33.1.6. Construct a nonlinear iteration function with Feigenbaum δ in the interval $2 < \delta < 4.6692\cdots$.

33.1.7. Determine the Feigenbaum δ for

(a) the exponential map of Exercise 33.1.1,

(b) some cubic map of Exercise 33.1.3,

(c) the time delayed logistic map of Exercise 33.1.4.

33.1.8. Find numerically the first four points μ for period doubling of the logistic map, and then obtain the first two approximations to the Feigenbaum δ. Compare with Fig. 33.3 and Eq. (33.7).

33.1.9. For the logistic map, find numerically values μ in the region $\mu > \mu_\infty$ where cycles of period 3, 4, 5, 6 begin and then where they become unstable.

Check values. For period 3, $\mu = 3.8284$,
4, $\mu = 3.9601$,
5, $\mu = 3.7382$,
6, $\mu = 3.6265$.

33.1.10. Consider the map $x_{n+1} = F(x_n)$ with

$$F(x) = \begin{cases} a + bx, & x < 1, \\ c + dx, & x > 1, \end{cases}$$

for $b > 0$ and $d < 0$. Show that its Lyapunov exponent is positive when $b > 1$ and $d < -1$. Plot a few iterations in the (x_{n+1}, x_n) plane.

33.2 PHASE SPACE

An understanding of the way in which dynamical systems evolve in time is facilitated by considering the concept of **phase space**, which has coordinates corresponding to the independent dynamical variables of the system. In mechanical systems these dynamical variables are normally chosen to be the components of the vectors describing the positions and momenta of the particles in the system, so, for example, the phase space of an N-particle system in 3-D space would have $6N$ dimensions. It is ordinarily possible to reduce the equations of classical mechanics to a coupled system of first-order differential equations; Hamilton's equations, Eq. (22.47), are of that form. Thus, the position and momentum of a particle at a given time corresponds to a particular point in phase space, and its trajectory (its time evolution) can be described by a path in phase space which can (in principle) be determined by solving a system of first-order ODE's in the single independent variable t (time). At this point it is important to note that because classical mechanics is deterministic, a knowledge of the values of all the relevant dynamical variables at a given time enables calculation of their values at all future times. In other words, this means that, given a phase-space point, the phase-space **trajectory** of the system from that point is completely determined.

A point in phase space may be a **fixed** (or **equilibrium**) point if at that point all the momentum coordinates are zero and the position coordinates are such that no net forces exist in the system. The trajectory then ends at the fixed point. If a phase-space point is not an equilibrium point, the time-reversal symmetry of classical mechanics dictates that the trajectory leading **to** it must also be unique. A main conclusion we can draw from these observations is that phase-space trajectories **cannot cross** and can only terminate at equilibrium points.

If we now consider the possible forms trajectories can take in a two-dimensional phase space (corresponding to a particle moving in one spatial dimension), we see that the possibilities are very limited: we can have fixed points, curves that end at or spiral toward or away from fixed points (without crossing each other), perhaps closed loops (which describe periodic orbits), or simply families of curves that neither terminate nor cross. But when our phase space has more than two dimensions, more complicated nonintersecting trajectories can, and do occur. Under suitable conditions these lead to an extremely strong dependence on initial conditions and the resulting chaotic motion is called **deterministic chaos**.

LIOUVILLE'S THEOREM

The **phase-space density** is an important concept with strong implications for dissipative systems. Apart from a normalization factor (that can be justified in quantum statistical mechanics but is arbitrary in classical mechanics), we can define relative density in phase space by considering a bundle of trajectories that are found within a differential phase-space volume at a given time, and ask what volume is required to contain them at future times. **Liouville's theorem** states that, for a conservative system (one without dissipative forces that can be described by a Hamiltonian), the **convective density** in phase space is a conserved quantity. This statement corresponds to the notion that our bundle of trajectories is contained in a phase-space volume that, although moving and perhaps distorted in shape, remains the same size.

If, however, our system contains dissipative forces (e.g., friction), then Liouville's theorem no longer holds and often our entire bundle of trajectories will move closer

together with time, perhaps finally completely collapsing into an equilibrium point. In this case, the phase-space density is increasing, reaching a singularity at the fixed point. It is this feature, and its opposite (phase-space dilatation) that are important for the study of chaos.

The proof of Liouville's theorem is not difficult. Letting $\rho(t)$ stand for the density of phase-space trajectories of a system at time t and at a phase-space point (p_i, q_i), where the p_i are the generalized momenta conjugate to the coordinates q_i, the change in density as the trajectories evolve is, applying the chain rule,

$$\frac{d\rho}{dt} = \frac{\partial\rho}{\partial t} + \sum_i \left(\frac{\partial\rho}{\partial p_i}\,\dot{p}_i + \frac{\partial\rho}{\partial q_i}\,\dot{q}_i \right) . \tag{33.13}$$

When the conditions for Liouville's theorem are satisfied, the right-hand side of Eq. (33.13) must evaluate to zero.

We proceed, assuming our phase-space point is not a fixed point, by noting that the continuity of trajectories implies that ρ must satisfy an equation of continuity, of the form

$$\frac{\partial\rho}{\partial t} + \sum_i \left(\frac{\partial(\rho\,\dot{p}_i)}{\partial p_i} + \frac{\partial(\rho\,\dot{q}_i)}{\partial q_i} \right) = 0 . \tag{33.14}$$

Expanding the derivatives in Eq. (33.14), we have

$$\frac{\partial\rho}{\partial t} + \sum_i \left(\frac{\partial\rho}{\partial p_i}\,\dot{p}_i + \rho\frac{\partial\dot{p}_i}{\partial p_i} + \frac{\partial\rho}{\partial q_i}\,\dot{q}_i + \rho\frac{\partial\dot{q}_i}{\partial q_i} \right) = 0 , \tag{33.15}$$

and subtracting the left-hand side of Eq. (33.15) from the right-hand side of (33.13) we reach

$$\frac{d\rho}{dt} = -\rho \sum_i \left(\frac{\partial\dot{p}_i}{\partial p_i} + \frac{\partial\dot{q}_i}{\partial q_i} \right) . \tag{33.16}$$

We now need to invoke the requirement that the system be conservative and that it can be described by a Hamiltonian. We may then use Hamilton's equations, Eq. (22.47), to replace $\dot{p}_i$ and $\dot{q}_i$ by derivatives of the Hamiltonian, according to

$$\dot{p}_i = -\frac{\partial H}{\partial q_i} , \qquad \dot{q}_i = \frac{\partial H}{\partial p_i} ,$$

so that Eq. (33.16) becomes

$$\frac{d\rho}{dt} = -\rho \sum_i \left(-\frac{\partial^2 H}{\partial p_i \partial q_i} + \frac{\partial^2 H}{\partial q_i \partial p_i} \right) = 0 . \tag{33.17}$$

Equation (33.17) establishes Liouville's theorem.

Example 33.2.1 Dissipation

Consider a particle of unit mass in free fall subject only to gravity, acceleration g. We use coordinates x and p which increase in the downward direction, and the equations of motion are

$$p(t) = p(0) + gt , \qquad x(t) = x(0) + p(0)t + gt^2/2 .$$

A region of phase space at time $t = 0$ (in this case an area) can be defined by the four points (x_1, p_1), (x_2, p_1), (x_1, p_2), (x_2, p_2). In general we would require the area to be

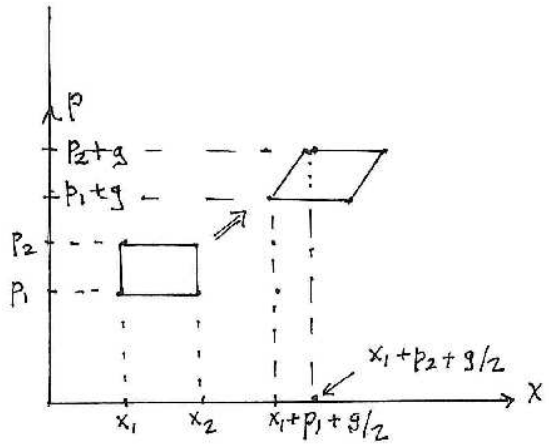

Figure 33.4: Evolution of phase-space area, Example 33.2.1.

infinitesimal ($x_2 = x_1 + dx$, $p_2 = p_1 + dp$), but the linearity of the present problem makes that unnecessary. This phase-space region is a rectangle with area

$$A(0) = (p_2 - p_1)(x_2 - x_1).$$

At $t = 1$, the four phase-space points have evolved as follows: $(x_1, p_1) \to (x_1 + p_1 + \frac{1}{2}g, p_1 + g)$, $(x_2, p_1) \to (x_2 + p_1 + \frac{1}{2}g, p_1 + g)$, $(x_1, p_2) \to (x_1 + p_2 + \frac{1}{2}g, p_2 + g)$, $(x_2, p_2) \to (x_2 + p_2 + \frac{1}{2}g, p_2 + g)$. These points form a parallelogram with base $x_2 - x_1$ and height $p_2 - p_1$, thereby causing the phase-space area to remain unchanged (see Fig. 33.4).

Now let's add air resistance to the dynamics, with the effect that $\dot{p} = g - kp$, with k a positive coefficient of friction. The result will be that during free fall the momentum approaches the terminal value g/k, and the detailed equations of motion become

$$p(t) = p(0)e^{-kt} + \frac{g}{k}\left(1 - e^{-kt}\right) , \qquad x(t) = x(0) + \frac{gt}{k} + \left(\frac{p(0)}{k} - \frac{g}{k^2}\right)\left(1 - e^{-kt}\right) .$$

These equations show that a phase-space area of initial width Δp in $p(0)$ will over time shrink to a width in p of zero, with time constant k, while an initial width Δx in x will, at constant $p(0)$, remain unchanged. The phase-space area will then decay to zero, corresponding to the fact that the dissipative force brings the momentum to the same terminal value irrespective of the initial conditions.

■

ANALYSIS OF PHASE SPACE

The phase-space trajectories of a dynamical system can be used as an indicator to determine whether the motion of that system is chaotic. However, for any system of real interest the phase space is of too great a dimension to make its trajectories easy to visualize, and there are two techniques that have been found helpful for that purpose. First, one can project the trajectories onto a plane; if the trajectory is periodic, so also will be its projection. The projected curves may have intersections, but these do not signify intersections of the actual trajectories, as the curves that intersect have

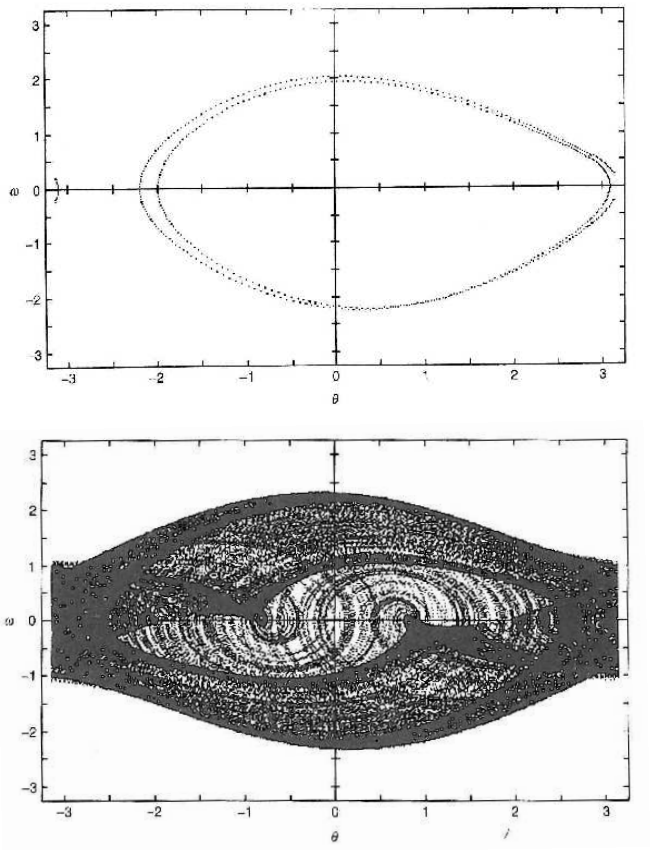

Figure 33.5: 2-D phase-space projections of (a) nonchaotic and (b) chaotic behavior. (From Baker and Gollub, *Chaotic Dynamics*, 2d ed.; used with permission of the copyright holder, Cambridge University Press.)

different values of at least one coordinate not in the plane of projection. Projected curves that are not periodic but neighboring at one point may remain neighboring as they travel on the plane of projection, but it is also possible that they deviate wildly from each other upon extension in time, and may even more or less densely fill entire regions of the projected space in a chaotic, or seemingly random manner. This is an indication of chaos. Figure 33.5 shows two phase-space projections; the first is neither periodic nor chaotic; the second exhibits chaotic behavior.

Another device for obtaining useful information from phase-space trajectories is to construct what are known as **Poincaré sections**. A Poincaré section is a plane located where it may be pierced by trajectories as they evolve in time, and the data thereby accumulated consists of the locations of the intersection points in the plane. Figure 33.6, in which the xy plane is chosen to be a Poincaré section and for simplicity the only additional phase-space coordinate shown is z, illustrates the schematics of the set-up. To gain a full understanding of a complicated system it may be advisable to construct a number of Poincaré sections, either parallel to each other at different values of some other coordinate(s) or at different orientations.

If a phase-space trajectory is periodic it will intersect a Poincaré section only a finite number of times. Chaotic trajectories will not only create an indefinitely

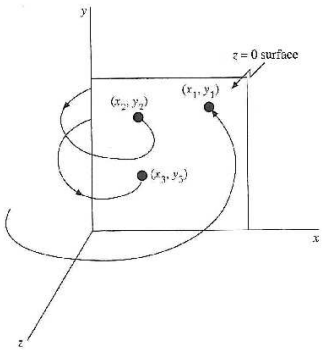

Figure 33.6: Schematic of a Poincaré section.

large number of intersections, but will typically create them in such a way that (if run for a long enough time) the intersections will form repeatedly interrupted curves that can be characterized as **self-similar**, meaning that their geometric patterns at least approximately repeat at progressively smaller scales. Patterns with this type of structure are termed **fractals**, and further study of them is the topic of Section 33.3. Nonchaotic and chaotic Poincaré sections are illustrated in Fig. 33.7.

Exercises

33.2.1. A particle of mass m is in oscillatory motion subject to a Hooke's law potential $V = kx^2$. The equations of motion for this system are

$$m\dot{x} = p\ , \qquad \dot{p} = -kx\ .$$

(a) Show that under time evolution, areas in phase space are preserved.

(b) Now add a friction force to the equation for $\dot{p}$ and show that the phase-space area of a given trajectory bundle shrinks to a point.

33.2.2. For the damped harmonic oscillator

$$\ddot{x} + 2a\dot{x} + x = 0,$$

consider the Poincaré section $\{x > 0, y = \dot{x} = 0\}$. Take $0 < a \ll 1$ and show that the map is given by $x_{n+1} = bx_n$ with $b < 1$. Find an estimate for b.

33.3 FRACTALS

In dissipative chaotic systems (but rarely in conservative Hamiltonian systems) new geometric objects with intricate shapes often appear that are called **fractals** because they have properties that lead to the introduction of an extended concept of **dimension** which for these objects assumes noninteger values. It is characteristic of fractals that their geometry exists at multiple scales, so their smaller parts resemble their larger parts. Intuitively a fractal is a set which is (either exactly or approximately) **self-similar** under magnification.

We need a quantitative measure of dimensionality in order to describe fractals. Unfortunately, there are several definitions with usually different numerical values,

none of which has yet become a standard. For strictly self-similar sets, one measure suffices. More complicated (for instance, only approximately self-similar) sets require more measures for their complete description. The simplest measure of dimensionality is the **box-counting dimension**, due to Kolmogorov and Hausdorff. For a one-dimensional set, we cover the curve by line segments of length R. In two dimensions the boxes are squares of area R^2, in three dimensions cubes of volume R^3, etc. Then we count the number $N(R)$ of boxes needed to cover the set. If we have, for example, a rope of length L (its important characteristic here is that the curve describing it is continuous and continuously differentiable), we would have as R is decreased

$$\lim_{R\to 0} R\,N(R) = L\ .$$

Similarly, for the 2-D region (with no holes) surrounded by a continuous and differentiable curve, we would define its area as the limit

$$\lim_{R\to 0} R^2\,N(R) = A\ .$$

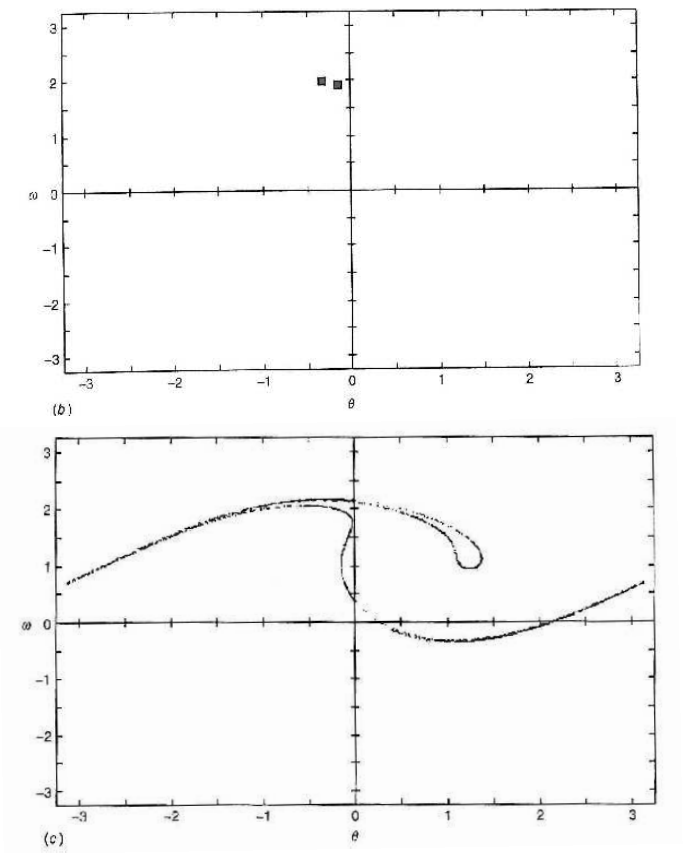

Figure 33.7: Poincaré sections for (a) nonchaotic and (b) chaotic behavior, same trajectories as in Fig. 33.5. (From Baker and Gollub, *Chaotic Dynamics*, 2d ed.; used with permission of the copyright holder, Cambridge University Press.)

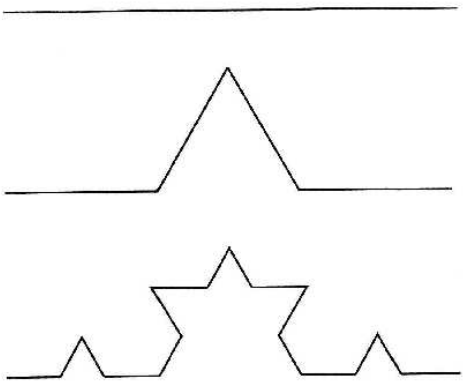

Figure 33.8: Koch curve (first two iterations).

These formulas are special cases of the relation

$$V_d = \lim_{R\to 0} R^d N(R) \ , \tag{33.18}$$

where d is the dimension of the space and V_d is the variable analagous to volume (length, area,...). Equation (33.18) can be rearranged to

$$\ln V_d = \lim_{R\to 0} \Big(d \ln R + \ln N(R) \Big) \ ; \tag{33.19}$$

Solving this equation for d and noticing that $\ln V_d$ becomes negligible in compariso to $\ln N(R)$, we reach the following formula for the **box-counting dimension**:

$$d = -\lim_{R\to 0} \frac{\ln N(R)}{\ln R} \ . \tag{33.20}$$

Our interest here is in sets that have properties such that the application of Eq. (33.20) will not yield integer values of d. As an initial example, consider a more irregular set, the **Koch** curve. We start with a line segment of unit length (see Fig. 33.8) and remove the middle third. Then we replace it with two segments of length 1/3, which form a triangular deviation to the line, as shown in the second panel of Fig. 33.8. We iterate this procedure with each segment ad infinitum; the first such iteration is the bottom panel of Fig. 33.8. The resulting Koch curve is infinitely long and is nowhere differentiable because of the infinitely many discontinuous changes of slope. At the nth step each line segment has length $R_n = 3^{-n}$ and there are $N(R_n) = 4^n$ segments. Hence its dimension is

$$d = -\lim_{n\to\infty} \left(\frac{n \ln 4}{-n \ln 3} \right) = \frac{\ln 4}{\ln 3} = 1.26\cdots \ ,$$

which is of greater dimension than a simple curve but less than that of a surface. Because the Koch curve results from iteration of the first step, it is strictly self-similar.

For the logistic map the box-counting dimension at a period-doubling accumulation point μ_∞ is $0.5388\ldots$, which is a universal number for iterations of functions in one variable with a quadratic maximum. To see roughly how this comes about,

consider the pairs of line segments originating from successive bifurcation points for a given parameter μ in the chaos regime (see Fig. 18.2). Imagine removing the interior space from the chaotic bands. When we go to the next bifurcation, the relevant scale parameter is $\alpha = 2.5029\ldots$ from Eq. (18.5). Suppose we need 2^n line segments of length R to cover 2^n bands. In the next stage then we need 2^{n+1} segments of length R/α to cover the bands. This yields a dimension $d = -\ln(2^n/2^{n+1})/\ln\alpha = 0.4498\ldots$. This crude estimate can be improved by taking into account that the width between neighboring pairs of line segments differs by $1/\alpha$ (see Fig. 18.2). The improved estimate, 0.543, is closer to 0.5388 .... This example suggests that when the fractal set does not have a simple self-similar structure, then the box-counting dimension depends on the box construction method.

Finally, we turn to the beautiful fractals that are surprisingly easy to generate and whose color pictures had considerable impact. For complex $c = a + ib$, the corresponding quadratic complex map involving the complex variable $z = x + iy$,

$$z_{n+1} = z_n^2 + c\ ,$$

looks deceptively simple, but the equivalent two-dimensional map in terms of the real variables

$$x_{n+1} = x_n^2 - y_n^2 + a\ , \qquad y_{n+1} = 2x_n y_n + b$$

reveals already more of its complexity. This map forms the basis for some of Mandelbrot's beautiful multicolor fractal pictures (we refer the reader to Mandelbrot (1989) and Peitgen and Richter (1986) in the Additional Readings), and it has been found to generate rather intricate shapes for various $c \neq 0$.

The **Julia set** of a map $z_{n+1} = F(z_n)$ is defined as the set of all its repelling fixed or periodic points. Thus it forms the boundary between initial conditions of a two-dimensional iterated map leading to iterates that diverge and those that stay within some finite region of the complex plane. For the case $c = 0$ and $F(z) = z^2$, the Julia set can be shown to be just a circle about the origin of the complex plane. Yet, just by adding a constant $c \neq 0$, the Julia set becomes fractal. For instance, for $c = -1$ one finds a fractal necklace with infinitely many loops (see Devaney in the Additional Readings).

Exercises

33.3.1. The **Cantor set** is formed from a line by removing its central 1/3, and then iterating an infinite number of times by removed the central 1/3 of each continuous segment that has survived earlier iterations. Find the box-counting dimension of the Cantor set.

33.3.2. Find the box-counting dimension of a fractal that is similar to the Cantor set, but with the central 1/2 iteratively removed from each continuous segment.

33.3.3. A two-dimensional set with an infinite number of square holes can be generated by carrying out the following process, starting from a unit square: (1) Divide the square into a 3×3 array of smaller squares, each of side 1/3 that of the original square; (2) Remove the central smaller square; (3) Repeat Steps 1 and 2 on each of the other smaller squares. Find the box-counting dimension of the resulting fractal.

33.4 AUTONOMOUS DIFFERENTIAL EQUATIONS

Differential equations that do not explicitly contain the independent variable are called **autonomous**. In typical mechanical systems, Hamilton's equations are of this type, so autonomous equations are important in physics. Letting the independent variable be t, a first-order autonomous equation takes the form

$$\dot{y} = f(y), \tag{33.21}$$

while for several dependent variables we have a system of equations

$$\dot{y}_i = f_i(y_1, y_2, \ldots, y_n), \quad i = 1, 2, \ldots, n. \tag{33.22}$$

Here the functions f_i are asssumed to be differentiable as needed.

Since our objective is to use autonomous equation systems for problems in mechanics, it is useful to consider the solutions of Eqs. (33.22) as defining phase-space trajectories, and to note that any phase-space points where all the f_i are simultaneously zero will be special, because they are points where all the positions and momenta will be stationary (and since all the position coordinates are stationary, the momenta must be zero). These points are termed **critical** or **fixed** points, and it is found that a local analysis of solutions to our autonomous system near the critical points leads to an understanding of the global behavior of the solutions. An important feature of such analyses is that they enable NDEs to be locally approximated by linear equation systems, which are much more easily handled.

As a preliminary example involving local linearization, let's look at Verhulst's ODE, $\dot{y} = \mu y(1-y)$, with $\mu > 0$. Here we have

$$f(y) = \mu y(1-y) = 0\,, \quad \text{with solutions } y = 0 \text{ and } y = 1.$$

To first order, in the neighborhood of $y = 0$, our ODE is $\dot{y} = \mu y$, with solution $y(t) = Ce^{\mu t}$. This solution indicates that (for either sign of C) $y(t)$ will diverge from zero as t increases, and (in keeping with nomenclature previously introduced) we identify $y = 0$ as a repellor (or a repellent critical point). A similar analysis for the neighborhhood of $y = 1$, where our ODE can be approximated as $\dot{y} = \mu(1-y)$, lead to the solution $y(t) = 1 - Ce^{-\mu t}$. In the limit of large t, $y(t)$ approaches 1 (the fixed point). We conclude that $y = 1$ is an attractor.

This ODE is simple enough that we can confirm our analysis by obtaining its exact solution. Because the equation is separable, we get

$$\int \frac{dy}{y(1-y)} = \int dy \left[\frac{1}{y} + \frac{1}{1-y}\right] = \ln \frac{y}{1-y} = \mu t + \ln C.$$

Hence $y(t) = Ce^{\mu t}/(1 + Ce^{\mu t})$, which for any C converges at $t \to \infty$ to unity, as predicted by our local analysis.

Continuing now to more general 1-D systems, we note that, for an arbitrary function f,

- in **one dimension**, fixed points y_i with $f(y_i) = 0$ divide the y-axis into dynamically separate intervals because, given an initial value in one of the intervals, the trajectory $y(t)$ will stay there, for it cannot go beyond either fixed point where $\dot{y} = 0$.

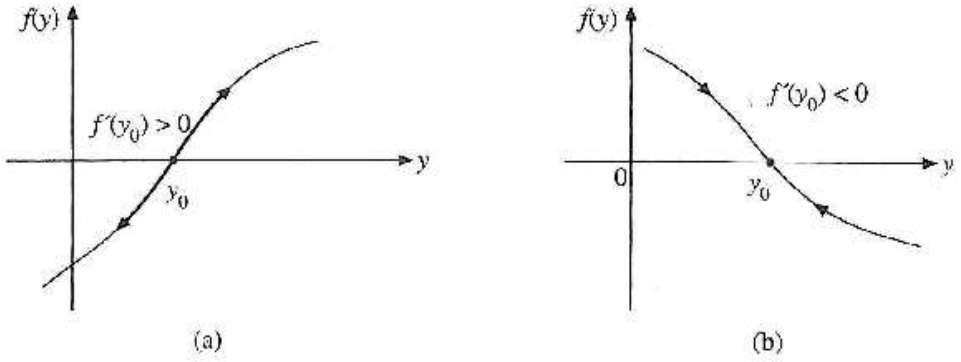

Figure 33.9: Fixed points: (a) repellor, (b) sink.

Next, we observe that if $f'(y_0) > 0$ at the fixed point y_0 where $f(y_0) = 0$, then at $y_0 + \varepsilon$ for $\varepsilon > 0$ sufficiently small, $\dot{y} = f'(y_0)\varepsilon + \mathcal{O}(\varepsilon^2) > 0$ in a neighborhood to the right of y_0, so the trajectory $y(t)$ keeps moving to the right, away from the fixed point y_0. To the left of y_0, $\dot{y} = -f'(y_0)\varepsilon + \mathcal{O}(\varepsilon^2) < 0$, so the trajectory moves away from the fixed point here as well. Hence,

- a fixed point [with $f(y_0) = 0$] at y_0 with $f'(y_0) > 0$, as shown in Fig. 33.9(a), repels trajectories; that is, all trajectories move away from the critical point; it is a **repellor**. Similarly, we see that

- a fixed point at y_0 with $f'(y_0) < 0$, as shown in Fig. 33.9(b), attracts trajectories; that is, all trajectories converge toward the critical point y_0; it is an **attractor**, also frequently called a **sink** or **node**.

Finally, we consider the remaining case when $f'(y_0) = 0$. Let us assume $f''(y_0) > 0$. Then at $y_0 + \varepsilon$, $\dot{y} = f''(y_0)\,\varepsilon^2/2 + \mathcal{O}(\varepsilon^3) > 0$, so the trajectory moves away from the fixed point, while if at $y_0 - \varepsilon$ it moves closer to y_0. This point is called a **saddle point**. For $f''(y_0) < 0$, the sign of $\dot{y}$ is reversed, so we deal again with a saddle point with the motion at $y_0 + \varepsilon$ toward the fixed point and at $y_0 + \varepsilon$ away from it. Let us summarize the local behavior of trajectories near such a fixed point y_0:

- If $f(y_0) = f'(y_0) = 0$, as shown in Fig. 33.10 for cases where (a) $f''(y_0) > 0$ and (b) $f''(y_0) < 0$, then trajectories on one side of y_0 converge toward it while those on the other side diverge from it. This type of critical point is a **saddle point**.

So far we have ignored the additional dependence of $f(y)$ on one or more parameters, such as μ in the Verhulst equation. When a critical point maintains its properties qualitatively as we adjust a parameter slightly, we call it **structurally stable**. This is a reasonable name; structurally unstable critical points are unlikely to occur in reality because noise and other neglected degrees of freedom act as perturbations on the system that effectively prevent such unstable points from being observed.

Let us now look at fixed points from this point of view. Upon varying such a control parameter slightly we deform the function f, or we may just shift f a bit up, down or sideways. Looking at both the graphs in Fig. 33.9, we see that this will cause a small shift in the location y_0 of the fixed point where $f(y_0) = 0$, but will maintain

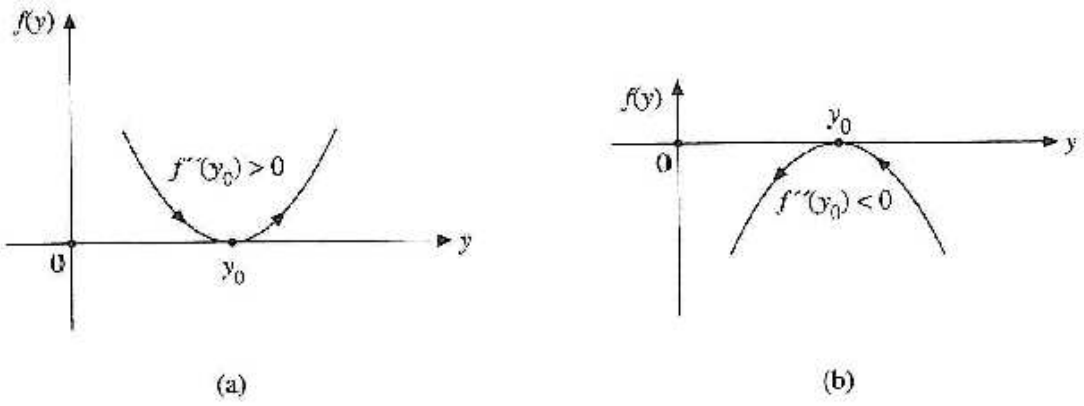

Figure 33.10: Saddle points.

the sign of $f'(y_0)$. Thus, both **sinks and repellors are structurally stable**. On the other hand, a small shift in a curve describing a saddle point has a qualitatively different effect. For example, shifting f in Fig. 33.10(a) down a bit creates two fixed points, one a sink and the other a repellor, and removes the saddle point. Shifting f up would have resulted in there being no fixed point in the vicinity. Since two conditions must be satisfied at a saddle point, they are not of frequent occurrence, and are of limited importance because of their instability with respect to variations of parameters. However, they mark a border between different types of dynamics and are useful and meaningful in global analyses. We are now ready to consider the richer, but more complicated, higher-dimensional cases.

LOCAL AND GLOBAL BEHAVIOR IN HIGHER DIMENSIONS

In two or more dimensions we start the local analysis at a fixed point $(y_1^0, y_2^0, \cdots)$ where, for each y_i, $\dot{y}_i = f_i(y_1^0, y_2^0, \cdots) = 0$. Each f_i is expanded in a Taylor series about the fixed point, retaining only the linear terms. This approach linearizes the coupled NDEs of Eq. (33.22). We abbreviate the derivatives at the fixed point as quantities f_{ij} defined as

$$f_{ij} \equiv \left.\frac{\partial f_i}{\partial y_j}\right|_{(y_1^0, y_2^0, \cdots)} . \tag{33.23}$$

Making also a change of notation to place the fixed point at the origin, we replace the y_i by $x_i \equiv y_i - y_i^0$, after which our newly linearized set of autonomous NDE's takes the form

$$\dot{x}_i = \sum_j f_{ij}\, x_j \ , \tag{33.24}$$

where it should be emphasized that the f_{ij} are constants, so our task is the relatively simple one of solving a set of first-order linear equations with constant coefficients.

A standard method for solving equation sets such as Eq. (33.24) is to make the Ansatz that the solution has the form

$$x_i(t) = \sum_j c_{ij}\, e^{\lambda_j t} \ , \tag{33.25}$$

where the c_{ij} and the λ_j are constants to be determined. The form of Eq. (33.25) is a straightforward generalization of the solutions found for single ODE's with constant coefficients in Section 7.3. Inserting Eq. (33.25) into Eq. (33.24) and carrying out the differentiation, we reach

$$\sum_j c_{ij}\,\lambda_j\,e^{\lambda_j t} = \sum_{jk} f_{ik}\,c_{kj}\,e^{\lambda_j t}\ . \tag{33.26}$$

These equations are linearly independent if no two of the λ_j are equal, and we limit further analysis to that case.[3] Having assumed that no two λ_j are equal, we see that Eq. (33.26) can only be satisfied for all t if it is separately satisfied for each j, so our problem reduces to the set of equations

$$\sum_k f_{ik}\,c_{kj} = \lambda_j\,c_{ij}\ , \qquad j = 1,\,2,\,\cdots\ . \tag{33.27}$$

But Eq. (33.27) can be cast as a matrix equation, with F a matrix of elements f_{ik} and $\mathbf{c}_j$ a column matrix with elements c_{ij}. In this notation, we have

$$\mathsf{F}\,\mathbf{c}_j = \lambda_j\,\mathbf{c}_j\ , \qquad j = 1,\,2,\,\cdots\ . \tag{33.28}$$

We now see that the λ_j are the eigenvalues of the matrix F and that the $\mathbf{c}_j$ are the corresponding eigenvectors. Note however that there is nothing in the definition of F that will guarantee that it be symmetric, Hermitian, or even normal, and there is therefore no requirement that the eigenvalues be real or that the eigenvectors be orthogonal.

Nevertheless, we may find the λ_j by solving the secular equation

$$\det\Big(\mathsf{F} - \lambda\mathbf{1}\Big) = 0\ , \tag{33.29}$$

after which we can solve for the eigenvectors $\mathbf{c}_j$, which we can then assemble (as columns) into a matrix that we call C. Then our solutions to Eq. (33.28) can be collected into the single equation

$$\mathsf{F}\,\mathsf{C} = \mathsf{C}\,\Lambda\ , \tag{33.30}$$

where Λ is a diagonal matrix containing the λ_j in the same order as that used to assemble the columns $\mathbf{c}_j$ into C. Remember that because F may not even be **normal**, C will not necesarily be unitary, but our current assumptions suffice to guarantee that it is not singular. Thus we can also write

$$\mathsf{C}^{-1}\mathsf{F}\,\mathsf{C} = \Lambda\ , \quad \text{and} \quad \mathsf{C}^{-1}\mathbf{x}(t) = e^{\Lambda t} \equiv \boldsymbol{\xi}(t) \quad \text{or} \quad \mathbf{x}(t) = \mathsf{C}\,\boldsymbol{\xi}(t)\ . \tag{33.31}$$

The latter two of these equations resulted from applying C^{-1} to Eq. (33.25) and writing $\mathbf{x}$ to stand for the column vector of elements x_i.

The new set of coordinates ξ_i (all of which are zero at the fixed point) have the property that

$$\dot{\xi}_i = \lambda_i \xi_i\ , \tag{33.32}$$

which means that the change in each ξ_i with time depends only on the corresponding λ_i, which is called a **characteristic exponent** of the fixed point. In other words,

[3] The so-called degenerate case where two λ_j are equal can be handled, but it requires special treatment that will not be discussed here.

the ξ_i are independent coordinates. If $\lambda_i > 0$, ξ_i will (if positive) increase with t and (if negative) become more negative as t increases, making the fixed point a repeller for the coordinate ξ_i. Conversely, if $\lambda_i < 0$, the fixed point will be an attractor for ξ_i. But because there is no requirement that λ_i be real, we can also have more complicated behavior that results when λ_i is complex.

To make the situation more concrete, this analysis has revealed that if our phase space is of dimension 2, a fixed point will be a sink in both dimensions if both $\lambda_1 < 0$ and $\lambda_2 < 0$, and a repellor in all directions if both $\lambda_1 > 0$ and $\lambda_2 > 0$. Other possibilities, including complex-valued λ_i, will be the subject of further discussion.

Example 33.4.1 Stable Sink

For this and later examples we write linear autonomous equations with a fixed point at the origin so as to eliminate the preliminary steps of expanding and linearizing the equation system and then changing coordinates to move the fixed point to the origin. For the present example, consider the following coupled ODEs:

$$\dot{x} = -x \ , \qquad \dot{y} = -x - 3y \ .$$

From $f_1 = -x$ we have $f_{11} = -1$, $f_{12} = 0$, while from $f_2 = -x - 3y$ we have $f_{21} = -1$ and $f_{22} = -3$. The secular determinant, Eq. (33.29),

$$\begin{vmatrix} -1-\lambda & 0 \\ -1 & -3-\lambda \end{vmatrix} = (1+\lambda)(3+\lambda) = 0,$$

yields the eigenvalues $\lambda_1 = -1$, $\lambda_2 = -3$. Because both are negative we have a stable sink at the origin. (We are now using the word **stable** to mean that we have a sink in all coordinates.)

Now that we have the characteristic exponents, we can write the general forms of x and y:

$$x(t) = c_{11}e^{\lambda_1 t} + c_{12}e^{\lambda_2 t} \ , \qquad y(t) = c_{21}e^{\lambda_1 t} + c_{22}e^{\lambda_2 t} \ .$$

We now substitute these expressions into the coupled ODEs:

$$\lambda_1 c_{11}e^{\lambda_1 t} + \lambda_2 c_{12}e^{\lambda_2 t} = -c_{11}e^{\lambda_1 t} - c_{12}e^{\lambda_2 t} \ ,$$

$$\lambda_1 c_{21}e^{\lambda_1 t} + \lambda_2 c_{22}e^{\lambda_2 t} = -c_{11}e^{\lambda_1 t} - c_{12}e^{\lambda_2 t} - 3c_{21}e^{\lambda_1 t} - 3c_{22}e^{\lambda_2 t} \ .$$

Equating coefficients of $e^{\lambda_i t}$ in these equations, and inserting the known values of the λ_i, we get

$$-c_{11} = -c_{11} \ , \quad -3c_{12} = -c_{12} \ , \quad -c_{21} = -c_{11} - 3c_{21} \ , \quad -3c_{22} = -c_{12} - 3c_{22} \ .$$

These equations show that $c_{12} = 0$, that c_{11} and c_{22} are arbitrary, and that $c_{21} = -c_{11}/2$. These data translate into

$$x(t) = c_{11}\, e^{-t} \ , \qquad y(t) = -\frac{c_{11}}{2}\, e^{-t} + c_{22}\, e^{-3t} \ .$$

In the limit $t \to \infty$, both x and y tend to zero, with $y \sim -x/2$. To find the orbit, we eliminate the independent variable, t, from the equation for y by substitution of e^{-t} from the formula for x:

$$y = -\frac{x}{2} + \frac{c_{22}}{c_{11}^3}\, x^3 \ .$$

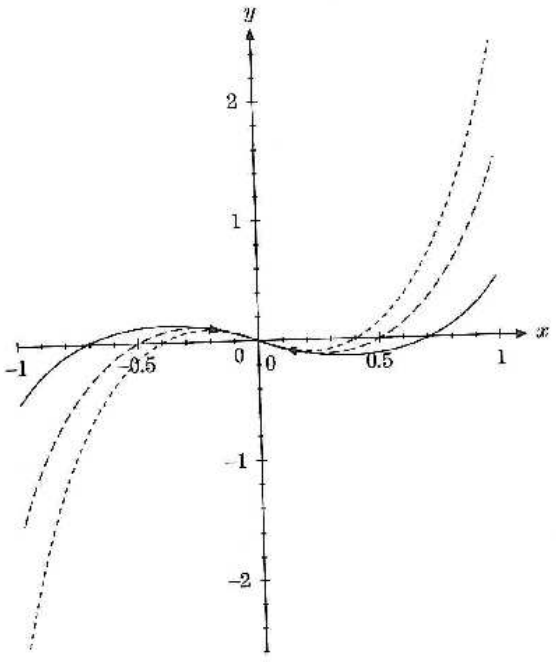

Figure 33.11: Stable sink.

Several orbits in the vicinity of the origin, with arrows marking the direction of the trajectories, are shown in Fig. 33.11.

■

Our next example is for a situation in which the characteristic exponents are not all of the same sign, so we have a sink in one dimension and a repellor in another, producing what in this context we call a **saddle point**.

Example 33.4.2 Saddle Point

Again we consider ODEs with a fixed point at the origin:

$$\dot{x} = -2x - y, \qquad \dot{y} = -x + 2y \ ,$$

with solutions of the form

$$x(t) = c_{11}\, e^{\lambda_1 t} + c_{12}\, e^{\lambda_2 t} \ , \qquad y(t) = c_{21}\, e^{\lambda_1 t} + c_{22}\, e^{\lambda_2 t} \ . \tag{33.33}$$

The characteristic exponents $\lambda = \pm\sqrt{5}$ are the eigenvalues of

$$\begin{vmatrix} -2-\lambda & -1 \\ -1 & 2-\lambda \end{vmatrix} = \lambda^2 - 5 = 0 \ .$$

Substituting Eq. (33.33) and the values of the λ_i into the ODEs yields the linear equations

$$\sqrt{5}\, c_{11} = -2c_{11} - c_{21} \ , \qquad \sqrt{5}\, c_{21} = -c_{11} + 2c_{21} \ ,$$

$$-\sqrt{5}\, c_{12} = -2c_{12} - c_{22}\, c_{12} \ , \qquad -\sqrt{5}\, c_{22} = -c_{12} + 2c_{22}\, c_{22} \ ,$$

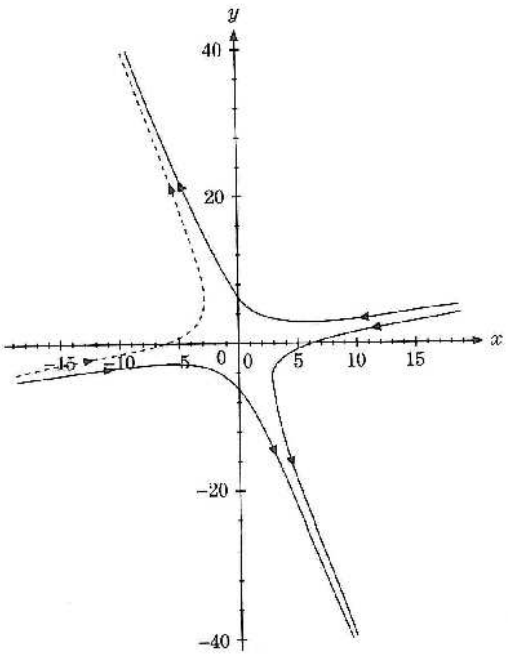

Figure 33.12: Saddle point.

with solutions $c_{21} = -(\sqrt{5}+2)\,c_{11},\ c_{22} = (\sqrt{5}-2)\,c_{12}$. The family of solutions depends on two parameters, $c_{11},\ c_{12}$. For the limit $t \to \infty$, the positive exponent prevails and $y \sim -(\sqrt{5}+2)x$, while for $t \to -\infty$ we have $y \sim (\sqrt{5}-2)x$. These straight lines are the asymptotes of the orbits. Because $-(\sqrt{5}+2)(\sqrt{5}-2) = -1$ they are orthogonal. We find the orbits by eliminating the independent variable, t. The result (see Exercise 33.4.1 for details) is

$$\frac{1}{5}(y+2x)^2 - x^2 = -4c_{12}c_{11} = \text{constant}. \tag{33.34}$$

This equation describes hyperbolic curves. However, they are at orientations that are oblique in the sense that their asymptotes (found earlier) are not aligned with the x and y axes. The four branches of the hyperbolas correspond to different choices for the signs of the parameters c_{11} and c_{12}. Figure 33.12 shows an orbit for the parameter values $c_{11} = \pm 1$, $c_{12} = \pm 2$.

■

We have previously observed that the characteristic exponents λ_i of our ODE systems may be complex. If the functions f_i in our ODEs are real (the usual case), the λ_i, if complex, must occur in conplex conjugate pairs, and thus will be of the form $\lambda_{1,2} = \rho \pm i\kappa$. this, in turn, means that the x_i for λ_1 and λ_2 will be linear combinations of $\exp(\rho t \pm i\kappa t)$, or the equivalent real forms $\exp(\rho t)\cos\kappa t$ and $\exp(\rho t)\sin\kappa t$. This functional dependence will cause the x_i to move on trajectories that circle about the fixed point, but spiraling toward it as t increases if $\rho < 0$, away from it if $\rho > 0$, and forming closed orbits in the special case $\rho = 0$. A fixed point with trajectories that spiral inward is called a **spiral node**, one with trajectories that spiral outward

is known as a **spiral repellor**, and one with trajectories that form closed orbits is called a **center** or a **cycle**.

Example 33.4.3 Spiral Fixed Point

Here is an example with a spiral fixed point at the origin. The coupled ODEs

$$\dot{x} = -x + 3y \ , \qquad \dot{y} = -3x + 2y$$

have solutions of the form

$$x(t) = c_{11}e^{\lambda_1 t} + c_{12}e^{\lambda_2 t} \ , \qquad y(t) = c_{21}e^{\lambda_1 t} + c_{22}e^{\lambda_2 t} \ , \tag{33.35}$$

in which the characteristic exponents λ_1, λ_2 are solutions of

$$\begin{vmatrix} -1-\lambda & 3 \\ -3 & 2-\lambda \end{vmatrix} = (1+\lambda)(\lambda-2) + 9 = \lambda^2 - \lambda + 7 = 0 \ .$$

The eigenvalues are complex conjugates with values $\lambda = 1/2 \pm i\sqrt{27}/2$, showing that we have a spiral fixed point (a repellor because the real part of λ is positive). Knowing the values of λ, we see that a convenient way to describe the solutions, instead of by Eq. (33.35), is as the trigonometric forms

$$x(t) = Ce^{t/2}\cos\kappa t \ , \qquad y(t) = e^{t/2}\Big[c_1 \sin\kappa t + c_2 \cos\kappa t\Big] \ , \tag{33.36}$$

By writing Eq. (33.36) we have arbitrarily fixed the phase of the x coordinate at $t = 0$ and given it the scaling C; this uses all our freedom to select a particular solution, and c_1 and c_2 will then have unique values. Note that we lose no important information about our system by our choice of the zero of time. The constant κ in Eq. (33.36) is the imaginary part of one of the two λ; we choose it to be $\kappa = \sqrt{27}/2$.

Differentiating the forms in Eq. (33.36) and substituting into the coupled ODEs, the ODE coefficients are found to satisfy the following four linear equations:

$$\tfrac{1}{2}\,C = -C + 3c_2 \ , \qquad -\kappa C = 3c_1 \ ,$$

$$\tfrac{1}{2}\,c_2 + \kappa c_1 = -3C + 2c_2 \ , \qquad -\kappa c_2 + \tfrac{1}{2}\,c_1 = 2c_1 \ .$$

The two equations on the top line can be solved simultaneously to yield $c_1 = -\kappa C/3$, $c_2 = C/2$. The two equations on the second line lead to the same result; this occurs because we used the characteristic exponents obtained from the secular equation.

In final form, our solutions are

$$x(t) = C\,e^{t/2}\,\cos(\sqrt{27}\,t/2) \ , \qquad y(t) = \frac{x}{2} - \frac{\sqrt{3}\,C}{2}\,e^{t/2}\,\sin(\sqrt{27}\,t/2) \ .$$

If we eliminate t from these equations we find the orbit:

$$x^2 + \frac{4}{3}\left(y - \frac{x}{2}\right)^2 = C^2\,e^t \ . \tag{33.37}$$

For fixed t this is the positive definite quadratic form $x^2 - xy + y^2 =$ constant, which is an ellipse. But the orbit is not an ellipse because t is not fixed, and the solution spirals out as t increases.

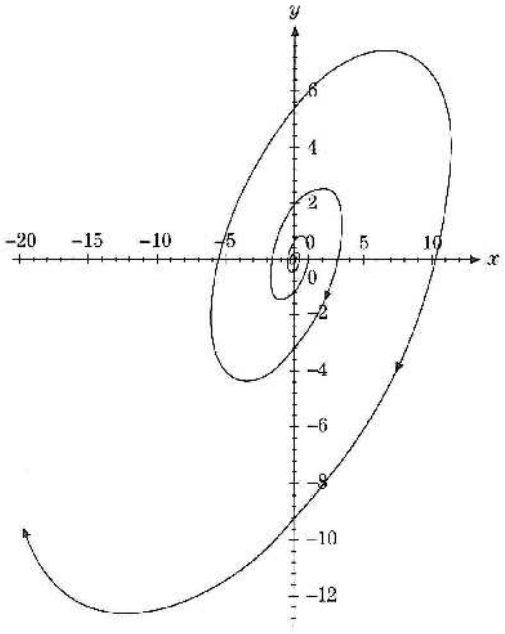

Figure 33.13: Spiral repellor.

It is of some interest to determine the orientation of the ellipse; that is the topic of Exercise 33.4.2, where the spiral is shown to be inclined from the vertical by 45°. See Fig. 33.13.

■

Our final example of behavior near a fixed point is a system of ODEs with a pair of pure imaginary characteristic exponents; as previously stated, this situation leads to circular orbits, the fixed point is called a **center**, and the closed orbits are termed **cycles**.

Example 33.4.4 Center Or Cycle

The undamped linear harmonic oscillator ODE $\ddot{x}+\omega^2 x = 0$ can be written as two coupled ODEs:

$$\dot{x} = -\omega y \ , \qquad \dot{y} = \omega x \ .$$

Proceeding by the methods of this section, we assume solutions of the form

$$x(t) = c_{11}e^{\lambda_1 t} + c_{12}e^{\lambda_2 t} \ , \qquad y(t) = c_{21}e^{\lambda_1 t} + c_{22}e^{\lambda_2 t} \ .$$

The characteristic exponents are found from the secular equation

$$\begin{vmatrix} -\lambda & -\omega \\ \omega & -\lambda \end{vmatrix} = \lambda^2 + \omega^2 = 0 = 0 \ .$$

with eigenvalues $\lambda = \pm i\omega$. Our ODEs have solutions (at a phase such that $y(0) = 0$)

$$x(t) = R\cos\omega t \ , \qquad y(t) = R\sin\omega t \ , \tag{33.38}$$

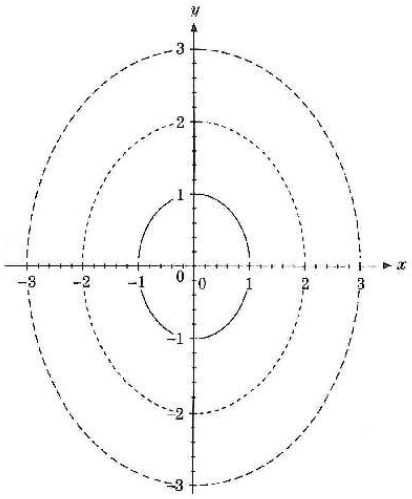

Figure 33.14: Center.

and these equations define the orbit $x^2 + y^2 = R^2$, namely a circle of radius R. Because the real parts of the characteristic exponents vanish, travel along the orbit can be in either direction; this corresponds to a change in the sign of ω in Eq. (33.38).

■

SUMMARY: BEHAVIOR NEAR FIXED POINTS

Because our analysis has been restricted to linearized equations, it cannot describe properties that are uniquely associated with nonlinearity (e.g., bifurations and chaos). But already we have encountered a wide variety of phenomena. Summarizing, we may have attractors (a.k.a. sinks, nodes), repellors, and fixed points of mixed character (attractor in some dimension(s), repellor in others). The approach to (or departure from) a fixed point may be radial, or it may be spiral. Systems may also have fixed points about which stable orbits can occur; such points are called **centers**. It is also possible to have stable quasiperiodic motion, corresponding to periodicity in two coordinates but with periods whose ratio is irrational.

In the presence of dissipation, trajectories may over time collapse into a state of equilibrium at rest at a fixed point, or may converge toward a closed orbit, which in that case is termed a **limit cycle**.

Exercises

33.4.1. Establish Eq. (33.34) for the orbit of the saddle-point trajectory of Example 33.4.2.

Hint. Start by obtaining $e^{-\lambda_1 t}$ and $e^{\lambda_2 t}$ separately in terms of x and y; then use the fact that $\lambda_2 = -\lambda_1$.

33.4.2. Establish the orientation of the ellipse defined by Eq. (33.37) if t is held constant.

33.4.3. Show that the (Rössler) coupled ODEs

$$\dot{x}_1 = -x_2 - x_3, \quad \dot{x}_2 = x_1 + a_1 x_2, \quad \dot{x}_3 = a_2 + (x_1 - a_3)x_3$$

(a) have two fixed points for $a_2 = 2,\ a_3 = 4$, and $0 < a_1 < 2$, and

(b) have a spiral repellor at the origin.

33.5 NONLINEAR DIFFERENTIAL EQUATIONS

In the introduction to this chapter we mentioned nonlinear differential equations (abbreviated as NDEs) as the natural place in physics for chaos to occur, but continued with the simpler iteration of nonlinear functions of one variable (maps). Here we briefly address the much broader area of NDEs and the far greater complexity in the behavior of their solutions. However, maps and systems of solutions of NDEs are closely related. As we pointed out in Section 33.2, we can use Poincaré sections to relate the behavior of solutions of an NDE to that of suitably chosen maps. This approach is particularly useful when solutions of NDEs are obtained numerically in computer simulations which can then be used to generate Poincaré sections. We then get relationships of the form

$$x_{n+1} = F_1(x_n, y_n), \qquad y_{n+1} = F_2(x_n, y_n)\ . \tag{33.39}$$

However, it may prove difficult to process these data in ways that permit explicit identification of the functions F_i as opposed to having the values of the F_i only at certain points.

In Section 33.4 we have seen how linearization of an NDE in the neighborhood of its fixed points can yield localized analyses that establish key features of its global behavior. In this final section of the present chapter we discuss briefly some specific NDEs and indicate features that may lead to solutions with chaotic behavior.

We have already encountered one NDE earlier in this book: the nonlinear Korteweg-deVries PDE, Eq. (9.24) , and its soliton solutions. Now we examine additional NDEs: the classical Bernoulli and Riccati equations.

BERNOULLI AND RICCATI EQUATIONS

Bernoulli equations are nonlinear, having the form

$$y'(x) = p(x)y(x) + q(x)[y(x)]^n, \tag{33.40}$$

where p and q are real functions and $n \neq 0,\ 1$ to exclude first-order linear ODEs. However, if we substitute

$$u(x) = [y(x)]^{1-n},$$

then Eq. (33.40) becomes a first-order linear ODE,

$$u' = (1-n)y^{-n}y' = (1-n)\Big[p(x)u(x) + q(x)\Big], \tag{33.41}$$

which we can solve (using an integrating factor) as described in Section 7.2.

Riccati equations are quadratic in $y(x)$:

$$y' = p(x)y^2 + q(x)y + r(x)\ , \tag{33.42}$$

where we require $p \neq 0$ to exclude linear ODEs and $r \neq 0$ to exclude Bernoulli equations. There is no known general method for solving Riccati equations. However, when a special solution $y_0(x)$ of Eq. (33.42) is known by a guess or inspection, then one can write the general solution in the form $y = y_0 + u$, with u satisfying the Bernoulli equation

$$u' = pu^2 + (2py_0 + q)u \ , \tag{33.43}$$

because substitution of $y = y_0 + u$ into Eq. (33.42) removes $r(x)$ from the resulting equation.

There are no general methods for obtaining exact solutions of most nonlinear ODEs. This fact makes it more important to develop methods for finding the qualitative behavior of solutions. In Chapter 7 we mentioned that power-series solutions of ODEs exist except (possibly) at essential singularities of the ODE. The coefficients in the power-series expansions provide us with the asymptotic behavior of the solutions. By making expansions of solutions to NDEs and retaining only the linear terms, it will often be possible to understand the qualitative behavior of the solutions in the neighborhood of the expansion point.

FIXED AND MOVABLE SINGULARITIES, SPECIAL SOLUTIONS

A first step in analyzing the solutions of NDEs is to identify their singularity structures. Solutions of NDEs may have singular points that are independent of the initial or boundary conditions; these are called **fixed singularities**. But in addition they may have **spontaneous**, or **movable**, singularities that vary with the initial or boundary conditions. This feature complicates the asymptotic analysis of NDEs.

Example 33.5.1 Moveable Singularity

Compare the linear ODE

$$y' + \frac{y}{x-1} = 0 \ ,$$

(which has an obvious regular singularity at $x = 1$), with the NDE $y' = y^2$. Both have the same solution with initial condition $y(0) = 1$, namely $y(x) = 1/(1-x)$. But for $y(0) = 2$, the linear ODE has solution $y = 1 + 1/(1-x)$, while the NDE now has solution $y(x) = 2/(1-2x)$. The singularity in the solution of the NDE has moved to $x = 1/2$.

■

For a linear second-order ODE we have a complete description of its solutions and their asymptotic behavior when two linearly independent solutions are known. But for NDEs there may still be **special solutions** whose asymptotic behavior is not obtainable from two independent solutions. This is another characteristic property of NDEs, which we illustrate again by an example.

Example 33.5.2 Special Solution

The NDE $y'' = yy'/x$ has two linearly independent solutions that define the two-parameter family of curves

$$y(x) = 2c_1 \tan(c_1 \ln x + c_2) - 1 \ , \tag{33.44}$$

where the c_i are integration constants. However, this NDE also has the special solution $y = c_3 =$ constant, which cannot be obtained from Eq. (33.44) by any choice of the parameters c_1, c_2.

The "general solution" in Eq. (33.44) can be obtained by making the substitution $x = e^t$, then defining $Y(t) \equiv y(e^t)$ so that $x(dy/dx) = dY/dt$, thereby obtaining the ODE $Y'' = Y'(Y + 1)$. This ODE can be integrated once to give $Y' = \frac{1}{2}Y^2 + Y + c$ with $c = 2(c_1^2 + 1/4)$ an integration constant. The equation for Y' is separable and can be integrated again to yield Eq. (33.44).

■

BIFURCATIONS IN DYNAMICAL SYSTEMS

A bifurcation is a sudden change in dynamics for specific parameter values such as the birth of a node-repellor pair of fixed points or their disappearance upon adjusting a control parameter; that is, the motions before and after the bifurcation are topologically different. At a bifurcation point, not only are solutions unstable when one or more parameters are changed slightly, but the character of the bifurcation in phase space or in the parameter manifold may change. Thus we are dealing with fairly sudden events of nonlinear dynamics. Rather sudden changes from regular to random behavior of trajectories are characteristic of bifurcations, as is sensitive dependence on initial conditions: Nearby initial conditions can lead to very different long term behavior. If a bifurcation does not change qualitatively with parameter adjustments, it is called **structurally stable**. Just as we previously observed for fixed points, structurally unstable bifurcations are unlikely to occur in reality because noise and other neglected degrees of freedom act as perturbations on the system that effectively eliminate unstable bifurcations from our view. Bifurcations (such as period doublings in maps) are important as one among many routes to chaos. Others are sudden changes in trajectories associated with several critical points called **global bifurcations**. Often they involve changes in basins of attraction and/or other global structures. The theory of global bifurcations is fairly complicated and is still in its infancy at present.

Bifurcations that are linked to sudden changes in the qualitative behavior of dynamical systems at a single fixed point are called **local bifurcations**. More specifically, a change in stability occurs in parameter space where the real part of a characteristic exponent of the fixed point alters its sign, that is, moves from attracting to repelling trajectories, or vice versa. The **center-manifold theorem** says that at a local bifurcation only those degrees of freedom matter that are involved with characteristic exponents going to zero: $\Re e\lambda_i = 0$. Locating the set of these points is the first step in a bifurcation analysis. Another step consists in cataloguing the types of bifurcations in dynamical systems, to which we turn next.

The conventional **normal forms** of dynamical equations represent a start in classifying bifurcations. For systems with one parameter (that is, a one-dimensional center manifold) we write the general case of NDE as follows

$$\dot{x} = \sum_{j=0}^{\infty} a_j^{(0)} x^j + c \sum_{j=0}^{\infty} a_j^{(1)} x^j + c^2 \sum_{j=0}^{\infty} a_j^{(2)} x^j + \cdots , \tag{33.45}$$

where the superscript on the $a^{(m)}$ denotes the power of the parameter c they are associated with. One-dimensional iterated nonlinear maps such as the logistic map of Section 33.1 (which occur in Poincaré sections) of nonlinear dynamical systems can

be classified similarly, viz.

$$x_{n+1} = \sum_{j=0}^{\infty} a_j^{(0)} x_n^j + c \sum_{j=0}^{\infty} a_j^{(1)} x_n^j + c^2 \sum_{j=0}^{\infty} a_j^{(2)} x_n^j + \cdots . \tag{33.46}$$

One of the simplest NDEs with a bifurcation is

$$\dot{x} = x^2 - c \, ,$$

which corresponds to all $a_j^{(m)} = 0$ except for $a_0^{(1)} = -1$ and $a_2^{(0)} = 1$. For $c > 0$, there are two fixed points (recall, these are at $\dot{x} = 0$); they are at $x_\pm = \pm\sqrt{c}$ and have characteristic exponents $2x_\pm$, so x_- is a node and x_+ is a repellor. For $c < 0$ there are no fixed points. Therefore, as $c \to 0$ the fixed point pair disappears suddenly; that is, the parameter value $c = 0$ is a repellor-node bifurcation that is structurally unstable.

A pitchfork bifurcation occurs for the the undamped (nondissipative and special case of the Duffing) oscillator with a cubic anharmonicity

$$\ddot{x} + ax + bx^3 = 0, \qquad b > 0.$$

It has a continuous frequency spectrum and is, among others, a model for a ball bouncing between two walls. When the control parameter $a > 0$, there is only one fixed point, at $x = 0$, a node, while for $a < 0$ there are two more nodes, at $x_\pm = \pm\sqrt{-a/b}$. Thus, we have a pitchfork bifurcation of a node at the origin into a saddle point at the origin and two nodes at $x_\pm \neq 0$. Another example of bifurcation (not even requiring introduction of a map) is a potential $V(x) = ax^2/2 + bx^4/4$, which posesses a single well for $a > 0$ but a double well (with a local maximum at $x = 0$) for $a < 0$.

When a pair of complex conjugate characteristic exponents $\rho \pm i\kappa$ crosses from a spiral node ($\rho < 0$) to a repelling spiral ($\rho > 0$) and periodic motion (a limit cycle) emerges, then we call the qualitative change a **Hopf bifurcation**. They occur in the quasiperiodic route to chaos that will be discussed in the next subsection.

In a global analysis we piece together the motions near various critical points, such as nodes and bifurcations, studying bundles of trajectories that flow more or less together in two dimensions. (This geometric view is the current mode of analyzing solutions of dynamical systems.) But this flow is no longer collective in the case of three dimensions, where trajectories diverge from each other in general, and the motion may become chaotic.

CHAOS IN DYNAMICAL SYSTEMS

Our previous summaries of intricate and complicated features of dynamical systems do not include chaos, although some of them, such as bifurcations, sometimes are precursors to chaos. In three- or more dimensional NDEs, chaotic motion may occur, often when a constant of the motion (an energy integral for NDEs defined by a Hamiltonian, for example) restricts the trajectories to a finite volume in phase space and when there are no critical points. Another characteristic signal for chaos is when for each trajectory there are others nearby, some of which move away from it, while others approach it with increasing time. The notion of exponential divergence of nearby trajectories can be made quantitative by computing Lyapunov exponents for Poincaré sections of the phase-space motion. In fact, this is a key method for studying

chaos. As one varies the location and orientation of the Poincaré plane, a fixed point on it often is recognized to originate from a limit cycle in the higher-dimension phase space. For example, attracting limit cycles show up as nodes in Poincaré sections, repelling limit cycles as repellors of Poincaré maps and saddle cycles as saddle points of those maps.

Three or more dimensions of phase space are required for chaos to occur because of the interplay of the necessary conditions we just discussed, viz.

- bounded trajectories (often the case for Hamiltonian systems),
- exponential divergence of nearby trajectories (guaranteed by positive Lyapunov exponents of corresponding Poincaré maps),
- no intersection of trajectories.

As we have already discussed, the last condition is obeyed by deterministic systems. A surprising feature of chaos, mentioned in the introductory paragraphs of this chapter, is how prevalent it is and how universal the routes to chaos often are, despite the overwhelming variety of NDEs.

An example for spatially complex patterns in classical mechanics is the driven planar pendulum, treated in detail by Baker and Gollub (Additional Readings).

Other good candidates for chaos are multiple-well potential problems,

$$\frac{d^2\mathbf{r}}{dt^2} + \boldsymbol{\nabla} V(\mathbf{r}) = F\left(\mathbf{r}, \frac{d\mathbf{r}}{dt}, t\right), \tag{33.47}$$

where F represents dissipative and/or driving forces. Another classic example is rigid-body rotation, whose nonlinear three-dimensional Euler equations are familiar, viz.

$$\begin{aligned} \frac{d}{dt} I_1\omega_1 &= (I_2 - I_3)\omega_2\omega_3 + M_1, \\ \frac{d}{dt} I_2\omega_2 &= (I_3 - I_1)\omega_1\omega_3 + M_2, \\ \frac{d}{dt} I_3\omega_3 &= (I_1 - I_2)\omega_1\omega_2 + M_3. \end{aligned} \tag{33.48}$$

Here the I_j are the principal moments of inertia and $\boldsymbol{\omega}$ is the angular velocity with components ω_j about the body-fixed principal axes. Even free rigid-body rotation can be chaotic, for its nonlinear couplings and three-dimensional form satisfy all requirements for chaos to occur. A rigid-body example of chaos in our solar system is the chaotic tumbling of Hyperion, one of Saturn's moons that is highly nonspherical. It is a world where the Saturn rise and set is so irregular as to be unpredictable. Another is Halley's comet, whose orbit is perturbed by Jupiter and Saturn. In general, when three or more celestial bodies interact gravitationally, chaotic dynamics is possible. Note, though, that computer simulations over large time intervals are required to identify this behavior in the solar system. For more details on chaos in such conservative Hamiltonian systems we refer to Chapter 8 of Hilborn in the Additional Readings.

ROUTES TO CHAOS IN DYNAMICAL SYSTEMS

Let us now look at some routes to chaos. The period-doubling route to chaos is exemplified by the logistic map in Section 33.1, and the universal Feigenbaum number δ is one of its quantitative features. Period doubling is common in dynamical systems. It may begin with limit-cycle (periodic) motion that shows up as a fixed point in a Poincaré section. The limit cycle may be associated with a node or some other fixed point. As a control parameter changes, the fixed point of the Poincaré map splits into two points; that is, the limit cycle has a characteristic exponent that may change sign, from attracting to repelling, causing the periodic motion to now have a period twice as long as before. We refer to Chapter 11 of Barger and Olsson in the Additional Readings for period-doubling plots of Poincaré sections for the Duffing oscillator with a periodic external force. Another example for period-doubling is a forced oscillator with friction (see the contribution by Helleman in the collection in the Additional Readings edited by Cvitanovic).

The quasiperiodic route to chaos is also quite common in dynamical systems, for example, starting from a time-independent fixed point. If we adjust a control parameter, the system undergoes a Hopf bifurcation to the periodic motion corresponding to a limit cycle in phase space. With further change of the control parameter, a second frequency appears. If the frequency ratio is an irrational number, the trajectories are quasiperiodic, eventually covering the surface of a torus in phase space; quasiperiodic orbits never close or repeat. Further changes of the control parameter may lead to a third frequency or directly to chaotic motion. Bands of chaotic motion can alternate with quasiperiodic motion in parameter space. An example for such a dynamic system is a periodically driven pendulum. Again, see Baker and Gollub, Additional Readings.

A third route to chaos goes via intermittency, where the dynamical system switches between two qualitatively different motions as its control parameters are changed. For example, at the beginning, periodic motion alternates with an occasional burst of chaotic motion. With a change of the control parameter, the chaotic bursts typically lengthen until, eventually, no periodic motion remains. The chaotic parts are irregular and do not resemble each other, but one needs to check for a positive Lyapunov exponent to demonstrate chaos. Intermittencies of various types are common features of turbulent states in fluid dynamics. The Lorenz coupled NDEs also show intermittency.

Exercises

33.5.1. Construct a Poincaré section for the Duffing oscillator given by the ODE

$$\ddot{x} + ax + bx > 3 = 0\,, \qquad b > 0.$$

Consider the cases $a > 0$, $a = 0$, and $a < 0$.

33.5.2. Consider the Riccati equation $y' = y^2 - y - 2$. A particular solution to this equation is $y = 2$. Find a more general solution.

33.5.3. A particular solution to $y' = -2xy^2 + x^2y - 1$ is $y = x^{-2}$. Find a more general solution.

33.5.4. Solve the Bernoulli equation $y' + xy = xy^3$.

33.5.5. ODE's of the form $y = xy' + f(y')$ are known as Clairaut equations. The first step in solving an equation of this type is to differentiate it, yielding

$$y' = y' + xy'' + f'(y')y'' , \qquad \text{or} \qquad y''\Big(x + f'(y')\Big) = 0 .$$

Solutions may therefore be obtained both from $y'' = 0$ and from $f'(y') = -x$. The so-called general solution comes from $y'' = 0$.

For $f(u') = (y')^2$,

(a) Obtain the general solution (note that it contains a single constant).

(b) Obtain the so-called singular solution from $f'(y') = -x$. By substituting back into the original ODE show that this singular solution contains no adjustable constants.

Note. The singular solution is the envelope of the general solutions.

33.5.6. Show that the (Rössler) coupled ODEs

$$\dot{x}_1 = -x_2 - x_3, \quad \dot{x}_2 = x_1 + a_1 x_2, \quad \dot{x}_3 = a_2 + (x_1 - a_3)x_3$$

have a spiral chaotic attractor for $a_1 = 0.398$.

Additional Readings

Amann, H., *Ordinary Differential Equations: An Introduction To Nonlinear Analysis.* New York: de Gruyter (1990).

Baker, G. L., and J. P. Gollub, *Chaotic Dynamics: An Introduction*, 2nd ed. Cambridge, UK: Cambridge University Press (1996).

Barger, V. D., and M. G. Olsson, *Classical Mechanics*, 2nd ed. McGraw-Hill (1995).

Bender, C. M., and S. A. Orszag, *Advanced Mathematical Methods For Scientists and Engineers.* New York: McGraw-Hill (1978), Chapter 4 in particular.

Bergé, P., Y. Pomeau, and C. Vidal, *Order within Chaos.* New York: Wiley (1987).

Cvitanovic, P., ed., *Universality in Chaos*, 2nd ed. Bristol, UK: Adam Hilger (1989).

Devaney, R. L., *An Introduction to Chaotic Dynamical Systems.* Menlo Park, CA: Benjamin/Cummings; 2nd ed., Perseus (1989).

Earnshaw, J. C., and D. Haughey, Lyapunov exponents for pedestrians. *Am. J. Phys.* **61**: 401 (1993).

Gleick, J., *Chaos.* New York: Penguin Books (1987).

Hilborn, R. C., *Chaos and Nonlinear Dynamics.* New York: Oxford University Press (1994).

Hirsch, M. W., and S. Smale, *Differential Equations, Dynamical Systems, and Linear Algebra.* New York: Academic Press (1974).

Infeld, E., and G. Rowlands, *Nonlinear Waves, Solitons and Chaos.* Cambridge, UK: Cambridge University Press (1990).

Jackson, E. A., *Perspectives of Nonlinear Dynamics.* Cambridge, UK: Cambridge University Press (1989).

Jordan, D. W., and P. Smith, *Nonlinear Ordinary Differential Equations*, 2nd ed. Oxford, UK: Oxford University Press (1987).

Lyapunov, A. M., *The General Problem of the Stability of Motion.* Bristol, PA: Taylor & Francis (1992).

Mandelbrot, B. B., *The Fractal Geometry of Nature.* San Francisco: W. H. Freeman, reprinted (1988).

Moon, F. C., *Chaotic and Fractal Dynamics*. New York: Wiley (1992).

Peitgen, H.-O., and P. H. Richter, *The Beauty of Fractals*. New York: Springer (1986).

Sachdev, P. L., *Nonlinear Differential Equations and their Applications*. New York: Marcel Dekker (1991).

Tufillar, N. B., T. Abbot, and J. Reilly, *An Experimental Approach to Nonlinear Dynamics and Chaos*. Redwood City, CA: Addison-Wesley (1992).